AIAA JOURNAL
Vol. 34, No. 2, February 1996

Cinematic Particle Image Velocimetry of High-Reynolds-Number Turbulent Free Shear Layer

Tom R. Oakley,* Eric Loth,† and Ronald J. Adrian‡
University of Illinois at Urbana–Champaign, Urbana, Illinois 61801

The objective of this research was to study the time-evolving velocity field in a two-stream, turbulent, planar free shear layer using a cinematic particle image velocimetry technique. The water shear layer had a velocity ratio of 0.23 and a Reynolds number of 2.62×10^4 based on velocity thickness and velocity difference. The cinematic particle image velocimetry system employed an argon-ion laser, a scanning mirror, and a 35-mm movie camera. Experimental data obtained by this technique yielded a combined spatial and temporal evolution of the two-dimensional velocity and spanwise vorticity fields. (The resulting set of 400 velocity vector fields is available by contacting the second author.) The detailed velocity field structure of the shear layer was significantly different from previous lower Reynolds number flow visualizations in that the classical well-defined eddies and braids were replaced with complex three-dimensional agglomerated vortices of both signs. The velocity field evolution was also notably different from that of the passive scalar field, where the former exhibited stronger temporal variations and reduced spatial coherency. Temporal and spatial correlations yielded transverse distributions of convection velocities based on both streamwise velocity perturbations and vorticity. Additionally, the spatial autocorrelation was performed to show the average eddy shape, and a Lagrangian tracking correlation method was used to estimate eddy lifetime.

Introduction and Previous Studies

MIXING layers, or free shear layers, have been the subject of intensive study for many years because of their importance to practical fluid dynamics and aerodynamics. The turbulent statistics of mixing layers (obtained primarily by hot wires) have been studied by several authors. Results for single-stream shear layers have been reported by Davies et al.,[1] Wygnanski and Fiedler,[2] and Batt,[3] to name a few. Two-stream shear layer results by Jones et al.,[4] Spencer and Jones,[5] Balint and Wallace,[6] and Foss and Haw[7] show statistical differences from single-stream or axisymmetric shear layers. The latter two of these are especially interesting, in that they present direct measurements of vorticity, which lends itself to comparison with the vorticity data derived from the present particle image velocimetry (PIV) velocity field data.

Early visualization studies of mixing layers by Brown and Roshko[8] showed that large-scale spanwise structures are still present and coherent at high Reynolds numbers ($\sim 10^5$). These large structures, called eddies and braids, provide the dominant entrainment mechanism for mixing layer flows. There have been many other investigations that have shown the manifestation, evolution, and dynamics of these structures in the entrainment process, whereby the underlying physics is governed by a three-dimensional unsteady motion with distinct vortex structures (for a discussion see Dimotakis[9]). Many of these studies documented the scalar transport dynamics (based on density fields or seeding the flow with a passive marker). However, there is a fundamental difference between statistics of passive scalar fields and turbulent velocity fields, primarily because of the historical nature of the former.[10] Therefore, it is of significant interest to obtain the spatio-temporal evolution of the velocity field for a free shear layer, which is the subject of this study.

PIV is a relatively new analysis technique that directly determines instantaneous velocity vectors for an entire plane of a flowfield simultaneously. Adrian[11] gives a review of the theory and advances in PIV, as well as other particle imaging techniques. One technique to obtain a high-resolution structured matrix of vectors is to apply correlations to small interrogation spots, which each contain several particle image pairs. A notable variation of the basic pulsed laser technique is to use a scanning laser beam, which increases the intensity of particle illumination available from a continuous wave (nonpulsed) laser.[12,13]

To the authors' knowledge there have been only two other studies that included velocimetry based on particle images for a planar free shear layer. Dimotakis et al.[14] used a variation of the PIV technique, particle streak velocimetry with digital processing, which was probably the first such application to free shear layers. The results centered on the appearance of negative velocities in the laboratory frame for a 1:6 velocity ratio. Recently, Post et al.[15] investigated a forced shear layer with particle tracking; however, the interrogation yielded nonuniform vector resolution that was low in the vortex cores, presumably due to the high Stokes numbers of the seed (~ 0.2). The study noted that the steepest gradients, i.e., maximum vorticity, occur at the vortex cores and not at the braids. The Reynolds numbers of these studies based on vorticity thickness, defined as the ratio of the overall shear layer velocity difference to the time-averaged vorticity at the centerline, were 2×10^3 and 5×10^2, respectively. The Reynolds number of the present study is more than one order of magnitude larger.

There have been only a few previous flow studies using time-resolved PIV with a film format, and these have typically employed drum cameras (with a limited number of frames per sequence) and particle tracking (which resulted in low unstructured resolution).[16,17] However, Lin and Rockwell[18] recently obtained images of the streamwise vorticity behind a cylinder using a 35-mm framing film camera and a single-frame cross-correlation PIV technique (which has many similarities with the present technique). Time-resolved digital PIV[19,20] offers several advantages over film-based cinematic PIV, primarily due to the removal of the analog-to-digital transfer step. However, typical spatial and temporal resolution of the image acquisition media are currently lower than potential film-based techniques for the same uncertainty levels.

Herein, we apply a film-based cinematic PIV system to a high-Reynolds-number turbulent free shear layer. Each velocity vector is based on correlations of typically 15 particle image pairs, which results in increased accuracy as opposed to single particle tracking. With the present technique, we have obtained a uniform high spatial resolution throughout the field of view (~ 27 vectors across

Presented as Paper 94-2298 at the AIAA 25th Fluid Dynamics Conference, Colorado Springs, CO, June 20–23, 1994; received Oct. 12, 1994; revision received April 7, 1995; accepted for publication April 21, 1995.

*Graduate Student, Department of Aeronautical and Astronautical Engineering. Student Member AIAA.

†Associate Professor, Department of Aeronautical and Astronautical Engineering. Senior Member AIAA.

‡Professor, Department of Theoretical and Applied Mechanics. Associate Fellow AIAA.

the velocity-based shear layer thickness δ). In addition, we retain high temporal accuracy: average convection between particle image pairs (used for velocity vectors) of $\sim\delta/60$ and average interframe convection of $\sim\delta/10$.

Experimental Methods

This experimental study was conducted in a closed-loop water tunnel with a total recirculation length of about 20 m and a 9:1 contraction ratio just upstream of the vertical test section and just downstream of a set of flow conditioners. The test section is ~0.7 m long with interior cross-section dimensions of 0.25 × 0.25 m. The unforced free shear layer is created by a splitter plate with pressure-correcting screens, similar to the one used by Dimotakis and Brown,[21] yielding a high-speed velocity (U_1) of 42.5 cm/s and a velocity ratio (U_2/U_1) of 0.23 (see Fig. 1). Further details of the flow facility may be found in Cebrzynski[22] and Oakley.[23]

At the above velocity ratio, no reverse flow was expected and none was observed, eliminating the need for directional bias correction or image shifting, which was confirmed in the PIV interrogated images. The movie camera field of view (FOV) was located from 52 to 64 cm downstream of the splitter tip. This downstream position was deemed sufficient for the flow to be fully developed, since it corresponded to roughly 1000 momentum thicknesses downstream.[8] In addition, the shear layer thickness δ, based on the transverse extent of 5 and 95% streamwise velocity values of the velocity difference (ΔU), yielded a Reynolds number based on δ (Re_δ) of roughly 2.6×10^4, which meets similar criteria given by Koochesfahani et al.[24]

The tracer particles used in this experiment were 8-μm hollow glass spheres made by Potters Industries, with specific gravity of 1.1 and a Stokes number of 1.5×10^{-5}. Illumination was provided by a 5-W argon-ion laser beam (operating all-lines, principal lines at 488 nm and 514 nm) scanning from a Lincoln Laser variable-speed, 24-sided polygonal mirror (see Fig. 1). The mirror rpm was set to allow three beam sweeps during the single frame open shutter time period of the movie camera. The use of a triple exposure serves to effectively increase the particle seeding density and increases the signal-to-noise ratio of the displacement peak in the correlation plane.[25] Triple pulsing also eliminates the need for precise synchronization between the scanning mirror and the movie camera, since any picture (or portion thereof) will be interrogatable as long as it at least has particle pairs. However, both the camera framing rate and the scanning mirror speed must remain constant, with the proper ratio.

After the light beam reflected off the scanning mirror, it passed through L_2, a 145-mm spherical lens with a focal length of 250 mm, designed to provide a uniform beam sweep width h of 122 mm perpendicular to the flow direction (see Fig. 1). The beam sweep angle from the polygonal mirror was 30 deg (twice the exterior angle),

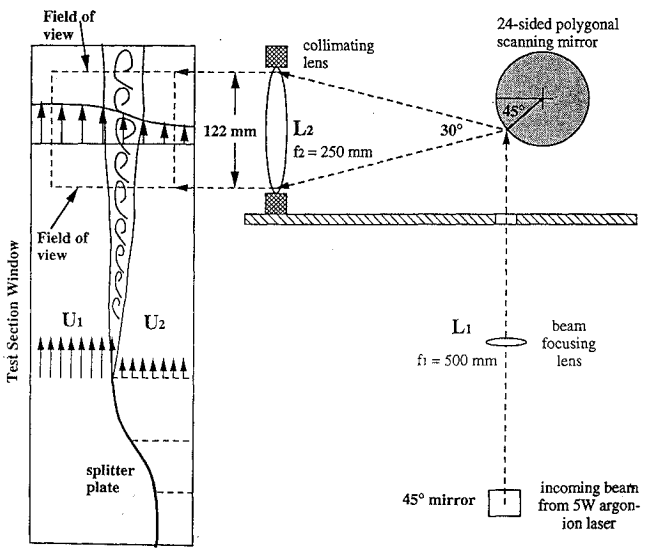

Fig. 1 Experimental schematic and optics arrangement with respect to the field of view.

so the $f\#$ of the collimating lens was chosen to match this angle and the desired parallel beam sweep width. Since an overly thin "sheet" would result in excessive loss of pairs due to significant out-of-plane motion,[25] a lens L_1 was used to adjust the thickness of the light sheet.

A Mitchell 35-mm variable-speed movie camera (which includes a double-pin register frame advancing mechanism) photographically recorded the triple exposures of the particles on film for subsequent PIV analysis. A feedback speed control unit, using an optical tachometer, was fabricated to provide a uniform framing rate to within 0.8%. The interframe temporal resolution of the results presented herein is 30 frames/second (fps). The time between sweeps ($\Delta t'$) is related to the frames/second based on the triple "pulse" character and a maximum angular rotating shutter opening of 170 deg. A Nikkor 60-mm focal length lens was used at a magnification M of 0.145 and a camera lens $f\#$ of 3.2. The images were recorded on Kodak black and white wide latitude surveillance 35-mm movie film, which has a nominal ASA rating of 400 and a maximum resolution of 125 lines per millimeter (lpmm). Because of the image orientation on movie film (designed to minimize the film transport speed), the actual exposed film area was limited to 25 × 19 mm for each frame.

To obtain both high spatial resolution and high flow Reynolds number Re_δ, δ was maximized by using both a small velocity ratio ($U_2/U_1 = 0.23$) and a large downstream distance x from the splitter plate tip. To balance the interest between convection dynamics and detailed spatial structure, the lengths of the FOV in the streamwise and transverse directions were set to be 122 and 129 mm, respectively, corresponding to a light "sheet" for each frame that was roughly 1.5 δ square. With an average shear layer velocity, $U_{av} \equiv (U_1 + U_2)/2$, of 0.26 m/s, a movie was taken to directly yield the spatio-temporal evolution of the velocity field.

PIV System Design

Although there is no single optimal set of parameters for PIV, the accuracy and utility of the experimental velocity data obtained can be maximized by careful consideration of the interaction among design variables. Desired spatial and temporal resolution imposes limits on the measurable range of flow speeds and the FOV dimensions (or vice versa), when considered along with hardware constraints and theoretical optical and PIV limitations. For cinematic PIV, the interest is on flowfield evolution, in addition to basic turbulence statistics, so the term adequate resolution is somewhat subjective. The goal of this study was to observe large-scale eddy dynamics with temporal resolution sufficient to track individual eddies as they convect downstream and clearly observe interaction between adjacent eddies, not to make measurements with the maximum spatial resolution. For statistics, limitation of the overall estimated errors in the measured velocity presents the most important objective constraint.

Test constraints include a specified mean velocity, velocity ratio, and shear layer thickness. The thickness determined the FOV, which in turn determined the magnification M for the given film size. The independent variables remaining include particle type, particle size d_p, movie camera framing rate (fps), film speed (ASA), film resolution H_{film} in lines per mm, camera lens focal length f, aperture ($f\#$), laser beam diameter in the field of view d_b, pulse separation interval $\Delta t'$, and interrogation spot size d_i. An additional constraint was given by the available argon-ion laser: a maximum power of 5 W and a wavelength λ of roughly 0.5 μ. Selection of the number of sides for the polygonal mirror and the variable-speed scanning frequency range were also chosen to allow future flexibility for possible increase of framing rate or extension of the velocity range to be studied.

For the several types of particles and films, a matrix of tests was completed to note actual image size d_τ and intensity on different film formats.[23] The results indicated the combination of the Potters microspheres and the Kodak surveillance film as the most suitable. To obtain preliminary resolution estimates, tests with the movie camera were completed to determine the image degradation as framing rate was increased. We define an overall resolution based on film resolution in lines per millimeter (H_{film}), camera lens resolution in

lines per millimeter (H_{lens}), degradation of resolution due to framing rate in lines per millimeter/frames per second (H_{fps}), digitizing charged-coupled device (CCD) lens resolution (using a magnification of 1:1) in lines per millimeter (H_{CCD}), and digitization resolution in pixels per d_i (H_d), yielding

$$\delta x = (1/H_{\text{film}} + 1/H_{\text{lens}} + \text{fps}/H_{\text{fps}} + 1/H_{\text{CCD}} + 2Md_i/H_d)/2 \quad (1)$$

Based on manufacturer specifications and resolution tests, H_{film} was estimated to be 80 lpmm, both lenses were each estimated to yield 150 lpmm, and H_{fps} was found to be 7850 lpmm/fps. This can be compared with the minimum particle image diameter on the film expected for infinite resolution, which is given by the diffraction limited spot size[11]:

$$d_e = \left[M^2 d_p^2 + 6f\#^2\lambda^2(1+M)^2\right]^{\frac{1}{2}} \quad (2)$$

Because of the resolution limitation, if δx is greater than d_e, then the actual image size on the CCD array will correspond to approximately δx, as opposed to d_e.

A complete theoretical discussion and Monte Carlo simulation results to assess the inherent limitations and necessary constraints for accurate PIV are given by Keane and Adrian,[26] with regards to cross-correlation PIV, and by Keane and Adrian,[25] with regards to multiple-pulsed systems. For cross correlation, the velocity gradient bias error is substantially reduced and can be eliminated by proper sizing and offset of the interrogation windows. To ensure a 95% probability of valid velocity detection, based on the preceding studies, we stipulated at least 15 particle pairs for cross correlation of a given interrogation spot. Further constraints included a maximum out-of-plane convection distance $\Delta z'$ of 0.25 d_b, a dimensionless velocity gradient with respect to the interrogation spot size (i.e., $M|\Delta \boldsymbol{u}|\Delta t'/d_I$) less than 0.03, a dimensionless velocity gradient with respect to the actual image size on film (i.e., $M|\Delta \boldsymbol{u}|\Delta t'/d_\tau$) less than 1.0, and a depth of field δz greater than d_b. We determined the maximum out-of-plane movement based on twice the expected peak rms values of spanwise velocity[2]: $\Delta z'_{\max} \sim 2(0.15)\Delta U \Delta t'$. Note that quantities associated with the time between two laser sweeps are denoted as ( )', and those between two movie frames as ( )''.

Full treatment of the errors associated with the finite film and digitization resolution is given by Prasad et al.[26] The total resolution-based error is shown to be the sum of a bias error, which decreases with increasing d_τ/d_{pix} (where d_τ is the actual image size on film, and d_{pix} is the pixel size), and a random error that increases linearly with d_τ/d_{pix}. Thus a minimum resolution-based error is obtained with an intermediate value of d_τ/d_{pix}. The value of the proportionality constant for the random error is a complex function of all of the nonideal aspects of the film, digitization, and the optics, so that an optimization is difficult. Because the algorithm used in this study uses curvefitting to obtain subpixel accuracy location of the correlation peak[28] (instead of the centroiding technique discussed by Prasad et al.[27]), the coefficient of the random error is conservatively estimated to be $c = 0.05$. For our value of $d_\tau/d_{\text{pix}} \approx 4$, the bias error was shown to be negligible, and so total rms resolution error equals the rms random error and is then 0.2 pixels. To determine the relative error, we must consider the range of displacements expected, e.g., $\Delta x'_{\max} = 1.1\Delta t' U_1$, and $\Delta x'_{\min} = 0.9\Delta t' U_2$, which correspond to 52.3 and 10.0 pixels, respectively. Thus, the relative errors are 0.3 and 2% for the high-speed and low-speed streams, respectively.

An additional error arises from the uncertainty of the rotating mirror speed. The desired rotational speed of 8.0 Hz could be set to within ±0.05 Hz, indicating an error of 0.6%. Another bias arises from the fact that for a scanning beam the time between exposures for any given particle is a function of its instantaneous speed.[12] This bias underestimates the instantaneous velocity by a maximum 1.7% in the high-speed stream, by 0.4% for the low-speed side, and by approximately 1% on the centerline.

All of the estimates of the various components of total velocity error discussed earlier can be combined to yield an overall uncertainty[29] that was minimized for the given constraints. The result was a nominal overall uncertainty for the instantaneous velocity of 1.8, 1.7, and 2.1% for the high, average, and low-speed portions of the shear layer, respectively.[23] For the current design, we note improvements in spatial and temporal shear layer resolution are primarily limited by the velocity uncertainty levels and the depth of field constraint (as magnification increases), where the velocity uncertainty level was principally determined by the relative uncertainty of the location of the displacement peak in the correlation plane in the low-speed region of the flow.

PIV Analysis

The processed film images were subsequently digitized by a CCD camera and subdivided into interrogation spots, which correspond to a 866-μm-square area on film. The interrogation algorithm is a highly efficient cross-correlation method developed by Keane and Adrian,[26] which extends the dynamic range of the velocimeter and takes advantage of an a priori knowledge of the mean flow. Two windows of dimension 128 × 128 pixels were cross-correlated to yield a single vector. A feature called trim automatically adjusts the streamwise window offset for maximum accuracy; this offset ranged from 12 to 48 pixels across the shear layer. The PIV interrogations were completed on a parallel digital processor system developed by Meinhart et al.,[28] which is capable of calculating over 100 vectors per second.

The resulting velocity vector components for each frame were obtained uniformly in both directions over a 43 × 41 matrix. Each vector is based on a 6.0-mm-square interrogation spot (physical), but 50% overlap is used, so that the physical vector spacing is 3.0 mm, or 3.75% of the shear layer velocity thickness δ. The temporal resolution of the velocity field evolution is given by $(U_{\text{av}}\Delta t'')/\delta = 0.11$, so that the large structures can easily be tracked between frames, and the distortion of eddies is seen as a gradual process. However, finer temporal resolution is needed to track smaller structures, i.e., tracking is limited to eddy sizes of order $\delta/10$.

The vorticity is calculated from the instantaneous velocity field by evaluating the circulation Γ around the square of the eight neighboring grid points and dividing by the enclosed area, $4\Delta x^2$ (Δx is the grid spacing). Thus, the uncertainty in vorticity combines the uncertainties of eight independent velocity vectors, i.e., $\Delta\omega = \sqrt{8}\Delta u/4\Delta x$, where $\Delta u \approx 0.016\Delta U$ is the maximum uncertainty in a given velocity vector. This results in a relative uncertainty (scaled by the mean vorticity, $\Delta U/\delta$) of the spatially averaged vorticity of 30%.

Flowfield Results

Preliminary dye visualization videos of the shear layer using the argon-ion laser and disodium fluorescein were first completed using a high dye concentration to mark the entire mixed fluid region; these results may be found in Cebrzynski[22] and Oakley.[23] Large-scale structures were observed, and the shear layer appeared to grow linearly from a virtual origin near the splitter tip.

Figures 2 and 3 show two portions of the PIV movie, each with a sequence of three consecutive frames of the processed velocity vectors, for which the average flow speed, U_{av}, has been subtracted to better highlight the turbulent structures, and the corresponding vorticity fields. The high-speed flow is on the left, the low-speed flow is on the right, and the flow is moving upwards as in Fig. 1. Each frame contains 1763 vectors, and the average convection upwards between frames is 2.9 vector spacings. The most remarkable aspect of these figures is the vortex structure complexity (both temporal and spatial) as compared with previous scalar or density based images.[8,30] The more rapid and pronounced changes of the velocity vectors associated with the large-scale structures as compared with their passive scalar counterparts is attributed to the historical dependence of the passive scalar field. For example, if the velocity field of an eddy suddenly becomes distorted, this will be immediately apparent in images of the velocity vectors. This explains why eddy life times based on velocity perturbations are less than those based on passive scalar perturbations.[3]

In general, these vector fields are also in stark contrast to the well-defined eddy and braid velocity vector fields obtained by Dimotakis et al.[14] for an Re_δ of $\sim 2.5 \times 10^3$ (as compared with the Re_δ of 2.62×10^4 for the present flow). The differences are even more exaggerated when compared with the results of Post et al.[15] for an Re_δ of $\sim 5 \times 10^2$. The differences are attributed to

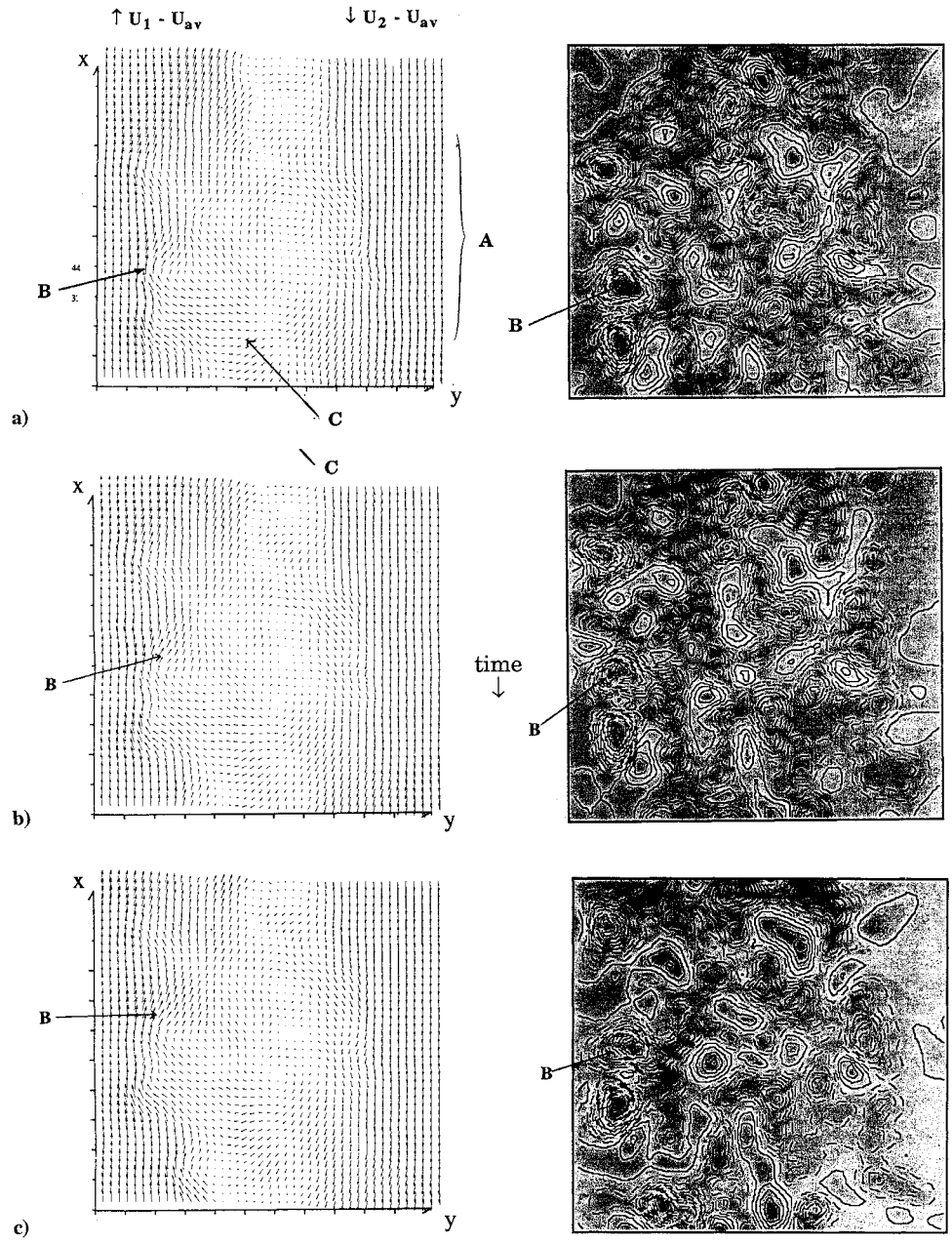

Fig. 2 Sequence of three frames showing both two-dimensional velocity vectors and spanwise vorticity. Flow is upwards and the average velocity U_{av} has been subtracted to highlight the vortex structures. Field of view dimensions are 122 mm in the x direction (streamwise) and 129 mm in the y direction (transverse).

the increased three-dimensionality, small-scale structures, and complexity of the present fully developed turbulent flow. Indeed, many computational fluid dynamic simulations of shear layers do not show such richness, indicating their inappropriateness for representing high-Reynolds-number unforced turbulent flows. However, recent DNS studies by Rogers and Moser[31] with shear layer visual thickness Reynolds numbers of up to 2×10^4 have shown complex small scales superposed on less coherent larger scale structures, similar to present results. Unfortunately, comparison of the present statistics with Rogers and Moser's high-Reynolds-number DNS is not directly possible, due to the temporally evolving nature of their study. One major conclusion of the Rogers and Moser study was that statistical and structural results of experiments are more closely matched by the simulations that did not exhibit organized pairings. The present results similarly argue that the simplified eddy/braid model with distinct pairing events is insufficient for describing some essential physics of shear layers.

The two sequences of Figs. 2 and 3 were selected in part due to their ability to represent the dynamics of the vortex merging. Examining the relative velocity vectors of Fig. 2, we note a large vortex (**A**) located in the center of the first frame with a size of about 80 mm ($\sim\delta$) across. Upon closer inspection, this vortex is seen to be composed of several smaller vortices, as well as two-dimensional sources and sinks due to spanwise variations of the velocity field (which were more easily discerned with the two-dimensional divergence field). Although this type of large-scale structure (**A**) has been noted in several previous flow visualization measurements, this level of smaller scale complexity is somewhat surprising and was found consistently through all 400 frames. This again points out why scalar fields, which may typically have recorded vortex **A** as a single structure of entrained fluid, can give a substantially different view of the flow turbulence.

In interpreting the velocity field, one must be careful not to presume points of zero relative velocity as vortex core centers, since convection speeds of eddies are known to fluctuate and vary as a function of transverse position.[3] For example, the perturbation (**B**) would reveal an eddy structure when a higher velocity is subtracted from the field. In fact, subtraction of the transverse distribution of the mean streamwise velocity revealed this structure as an eddy, but other previously identified eddies were lost as a result.[23] This

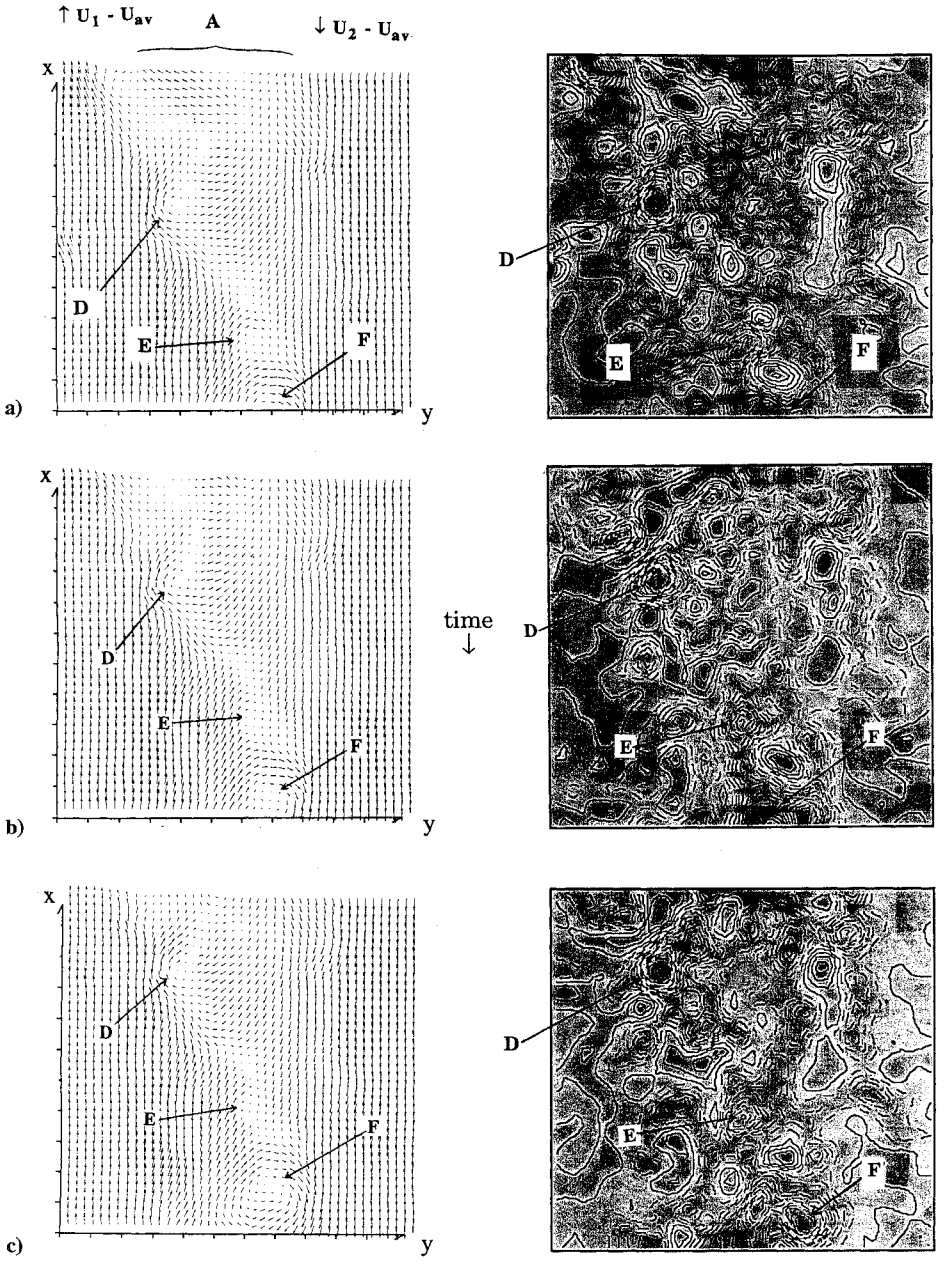

Fig. 3 Same caption as Fig. 2 except different sequence (beginning six frames after Fig. 2c).

indicates a variation of convection speeds at common transverse positions, such that comparison with the corresponding vorticity fields is important, e.g., it is easier to track structure **B** in the vorticity field.

One may also examine the juxtaposition of neighboring velocity vectors in Figs. 2 and 3, especially near vortex centers, and note that there are distinct regions where the flow does not appear divergence free, indicating either significant three-dimensionality of the flow and/or errors introduced by high local gradients. Based on estimated velocity uncertainties and previous studies,[32] three-dimensionality is primarily responsible. For the two-dimensional vector fields of this study, the spanwise velocity gradient can be calculated using incompressibility, i.e., $\nabla \cdot \boldsymbol{V} = 0$. This gives $-\partial w/\partial z = \partial u/\partial x + \partial v/\partial y$ [where $u(x, y)$ and $v(x, y)$ are the direct PIV results], which is an indicator of the three-dimensionality of the nominally two-dimensional (planar) shear layer. A sample instantaneous divergence map, which corresponds to Fig. 3c, is shown in Fig. 4. The dashed contour lines in a diagonal swath from upper left to lower right correspond to high divergence values of one sign along the braid region between two large eddies in the velocity vector map. This three-dimensionality is consistent with the low-Reynolds-number evolutions of shear layers of Lasheras and Choi,[32] where stream-

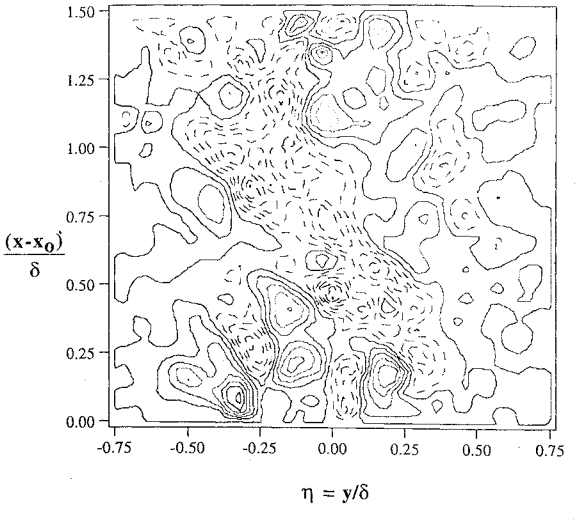

Fig. 4 Instantaneous divergence map corresponding to Fig. 3c.

wise vorticity would yield a strong upwash or downwash along braid regions.

The vorticity sequence of Fig. 2 displays the complexity of the shear layer structure at corresponding times, where strong temporal changes are noted to occur even in the Lagrangian frame. The dashed contour lines indicate regions of negative vorticity, whereas solid lines enclose positive vorticity. At this resolution, there is little evidence of the classic single point vortex model of only one sign. In addition, the sequence shows strong deviations in vorticity within small proximities, not observed in low-Reynolds-number shear layers.[15] The overall convection of the high vorticity regions indicates strong transverse variations in mean speed, local rotational events, and local straining events. We may note that structure (**B**) is now identified as a high vorticity region, further evidence of the variable convection speed of vortices throughout the shear layer.

Figure 3 (which begins six frames after Fig. 2c) is also of significance in that some evidence of vortex merging is seen in both the vector and vorticity fields. Examining the first frame, we note three eddy structures (**D–F**) that appear to be in the large braid region below the large vortex structure **A**, which has since convected upwards. By the second frame, eddy **E** has already lost some of its integrity and appears to be stretched along the braid between eddies **D** and **F**. By the third frame, it appears to have been strained further, causing a significant loss of coherency, and is gone within two more frames, leaving an enhanced eddy **F**. This phenomenon involving eddy destruction have been termed tearing by Hernan and Jimenez,[30] where it was observed to occur infrequently for the large-scale structures. This is not the classical merging, suggested by inviscid vortex amalgamation, i.e., rotational pairing until the cores coincide. Although there was evidence of some eddies grouping together to yield larger eddies, e.g., eddy **A**, this "destruction" of a weaker eddy to enhance a stronger eddy was noted frequently in the 400 frames processed.

With regard to resolution, the Taylor microscale of the flow was estimated at 3.2 mm, which is approximately equal to the vector spacing and thus one-half the interrogation spot size. However, the smallest scale of the flow is the Kolmogorov scale (estimated at 0.12 mm based on an expression for the dissipation given by Foss and Haw[7]), which is approximately 1/25 of the vector spacing. For comparison, the ratios of probe size to Kolmogorov scale in the experiments by Foss and Haw[7] and Balint and Wallace[6] are six and seven, respectively. Therefore, the vorticity fields presented herein are fundamentally underresolved and thus underestimate the magnitudes of vorticity peaks.

Statistical Results

Mean statistics of the 400 frames of velocity vectors were completed to determine the basic description of the flowfield. The first three such figures (Figs. 5–7) are used to evaluate the technique's ability to predict conventional shear layer statistics. The mean streamwise velocity profile is shown in Fig. 5, which resembles the characteristic hyperbolic tangent shape as expected. From this profile, the mixing layer thickness δ of 80 mm was determined, based on the 5% ΔU deviations from the two freestream velocities. The vorticity thickness, $\delta_\omega = \Delta U/(\partial U/\partial y)_{\max}$, was determined to be 71 mm. Although this parameter showed negligible growth within FOV, comparison to Brown and Roshko's[8] survey of uniform density mixing layer spread rates as a function of velocity ratio shows that it is well within the unforced growth rate range, assuming the virtual origin is at the splitter plate tip. Figure 6 shows the mean vorticity profile, calculated from the instantaneous vorticity fields (which are derived from the velocity fields, then line averaged). There is some deviation in the peak values in comparison with other two-stream data from Balint and Wallace[6] and Foss and Haw,[7] but in general the results are similar.

The rms values of the streamwise and transverse velocity components normalized by ΔU are shown in Fig. 7 as a function of transverse location from the centerline normalized by δ. These were obtained by first determining a mean velocity at each individual transverse and streamwise position by averaging over the 400 frames. Both peak values are low compared with the previous two-stream shear layer studies. We note that spatial averaging (due to interrogation spot size), interpolated vectors (more likely in high

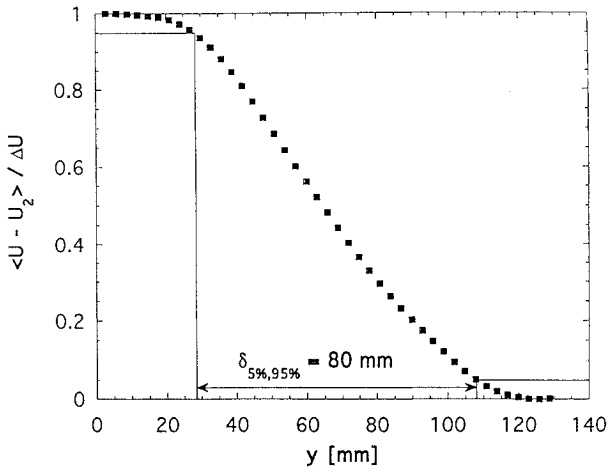

Fig. 5 Mean velocity profile based on average of 400 frames of PIV data. The mixing layer width is based on the 5 and 95% levels of ΔU.

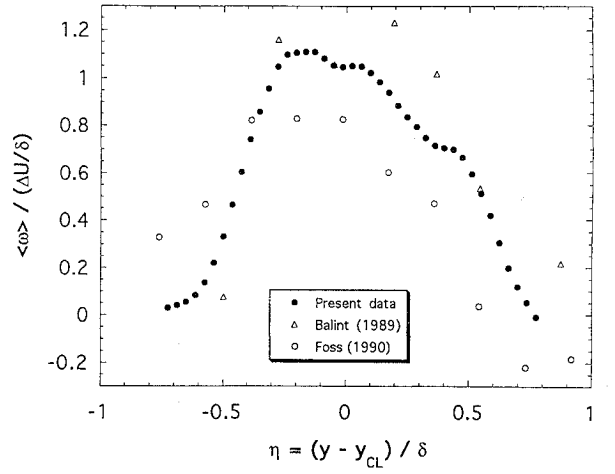

Fig. 6 Nondimensional mean vorticity profile.

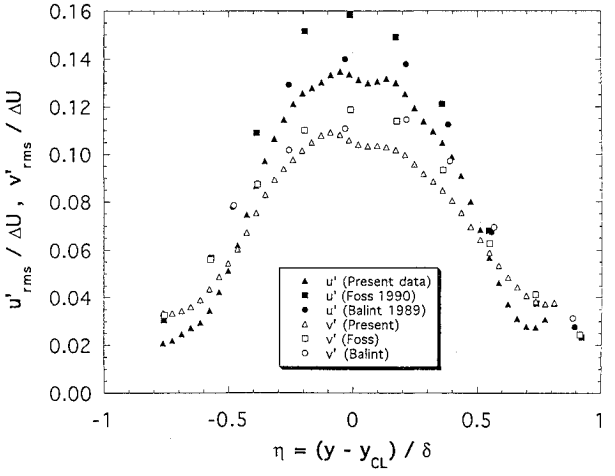

Fig. 7 Root-mean-square values of streamwise and transverse velocity fluctuations.

gradient regions), and finite data sampling (only 400 values to define the mean) will all reduce the rms levels of a field and can be a concern for PIV measurements when applied to statistics of highly turbulent flow.

In general, the streamwise velocity perturbations are the strongest as compared with the transverse and spanwise perturbations[2] and thus typically contain the highest signal-to-noise ratio. Therefore, many investigations of the turbulence structure of shear layers have examined correlations of the streamwise velocity perturbations through time and/or space. Such correlations have been obtained with hot wires, hot film probes, and laser-Doppler velocimetry, but

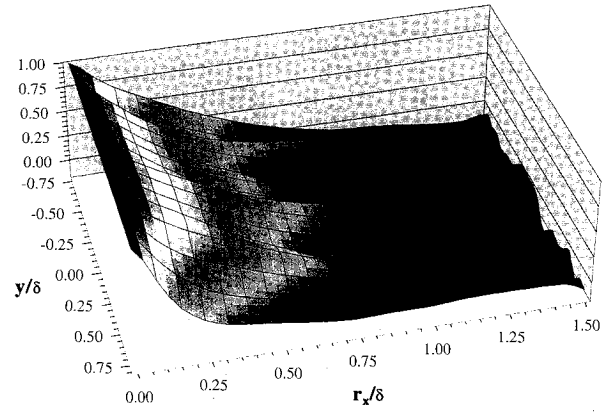

Fig. 8 Spatial correlation $R_{u'u'}(r_x, 0, y, 0)$ of streamwise velocity fluctuations as a function of nondimensional transverse location and streamwise shift.

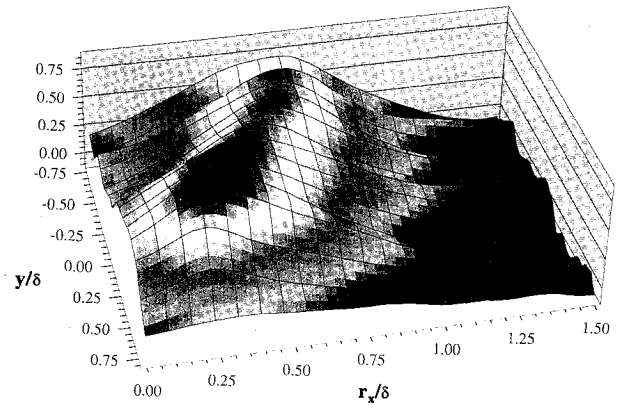

Fig. 9 Time-shifted spatial correlation of streamwise velocity fluctuations $R_{u'u'}(r_x, 0, y, \tau)$ with fixed time lag of 133 ms $[\tau/(\delta/\Delta u) \sim 0.5]$ as a function of nondimensional transverse location and streamwise shift.

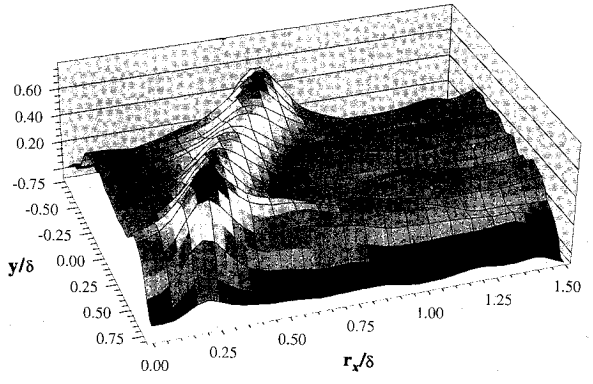

Fig. 10 Time-shifted spatial correlation of vorticity $R_{\omega\omega}(r_x, 0, y, \tau)$ with fixed time lag of 133 ms $[\tau/(\delta/\Delta u) \sim 0.5]$ as a function of nondimensional transverse location and streamwise shift.

the authors are unaware of the use of PIV to obtain such correlations in a turbulent free shear layer.

We define a general spatio-temporal correlation of the streamwise velocity perturbation (u') as

$$R_{u'u'}(r_x, r_y, y, \tau) = \langle u'(x, y, t)u'(x+r_x, y+r_y, t+\tau)\rangle / \langle u'_{\text{rms}}(y)^2\rangle \tag{3}$$

where $\langle \cdots \rangle$ indicates a spatial and temporal average over all available data samples of the 400 frames, and τ is restricted to integral multiples of the interframe time interval $\Delta t''$. The spatial correlation $R_{u'u'}(r_x, 0, y, 0)$ is shown in Fig. 8 as a function of the transverse position across the shear layer, where we may note significant transverse variations in the amplitude and shape of the correlation. For example, the centerline first decreases smoothly but then returns to a strong positive correlation peak, indicating the average vortex spacing at this transverse location. Near the shear layer edges, the correlation tends to reduce more slowly, presumably due to the reduced evolutionary behavior at these points (correlate with vorticity contours of Figs. 2 and 3). The general shape of this correlation compares well with results by Wygnanski and Fiedler[2] and others, although previous investigations typically have not carried out the correlation as far downstream. The average spatial extent of this correlation can be estimated by calculation of the integral length scale Λ, defined as follows:

$$\Lambda_{u'u'}(y) = \int_0^\infty R_{u'u'}(r_x, 0, y, 0)\, dr_x \tag{4}$$

The integral length scale results are presented in Oakley.[23] The length scale magnitudes were comparable to other two-stream shear layers (e.g., Jones et al.[4]), but notably lower than single-stream integral length scales. The reason for this difference is not clear at present.

The time-shifted spatial correlation $R_{u'u'}(r_x, 0, y, \tau)$ is shown in Fig. 9, where τ was fixed at $4\Delta t''$ [where $\tau/(\delta/\Delta U) \approx 0.55$, approximately the average Eulerian integral time scale of the present flow]. Here we note that the peak correlation reaches a value of about 3/4 within the shear layer but is lower outside of the shear layer especially for the low-speed side. This indicates that perturbations extending this far from the centerline are short lived, presumably related to momentary excursions of eddy trajectories into these otherwise nonturbulent regions. This is consistent with the dropoff of integral scale for transverse positions outside of δ as can be inferred from Fig. 8. Figure 10 shows a similar correlation (analagous to Fig. 9) using the instantaneous vorticity in place of u' in Eq. (3), i.e., $R_{\omega\omega}(r_x, 0, y, \tau)$. To the best of the authors' knowledge, this correlation has not been shown before. Comparison of Figs. 9 and 10 shows similar correlation shapes and magnitudes, but the correlation of vorticity has a much narrower peak. This is because the highest vorticity (i.e., most significant contributor to the correlation) is concentrated in small-scale structures considerably smaller than Λ (see Figs. 2 and 3), instead of having a smooth distribution over a scale

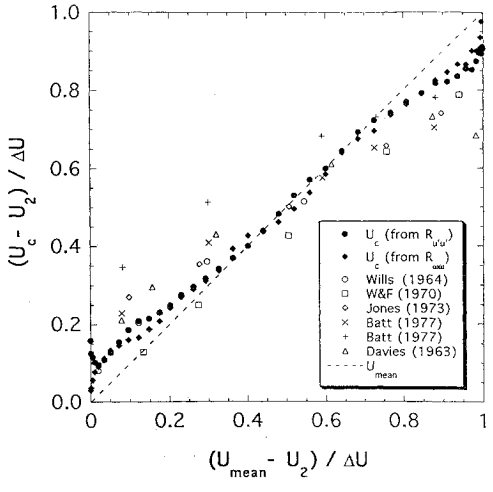

Fig. 11 Normalized distribution of convection speed U_c based on $R_{u'u'}(r_x, 0, y, \tau)$ and $R_{\omega\omega}(r_x, 0, y, \tau)$ as a function of mean velocity (Fig. 5).

$\sim\Lambda$. Therefore, the autocorrelation is much more localized for ω than for u' (see Fig. 12).

Taking the r_x at the peak correlation value as a function of transverse position from both the correlations of u' and ω, one may obtain the convection speed (U_c) of the most energetic streamwise velocity perturbations and strongest vorticity values, respectively. Figure 11 shows the combined convective velocity curves based on u' and ω, in comparison with previous experimental data. The curves of the present study agree quite well with each other, and their trend is in agreement with that shown by other researchers, i.e., $U_c < U(y)$ near the high-speed stream and $U_c > U(y)$ near the low-speed stream.

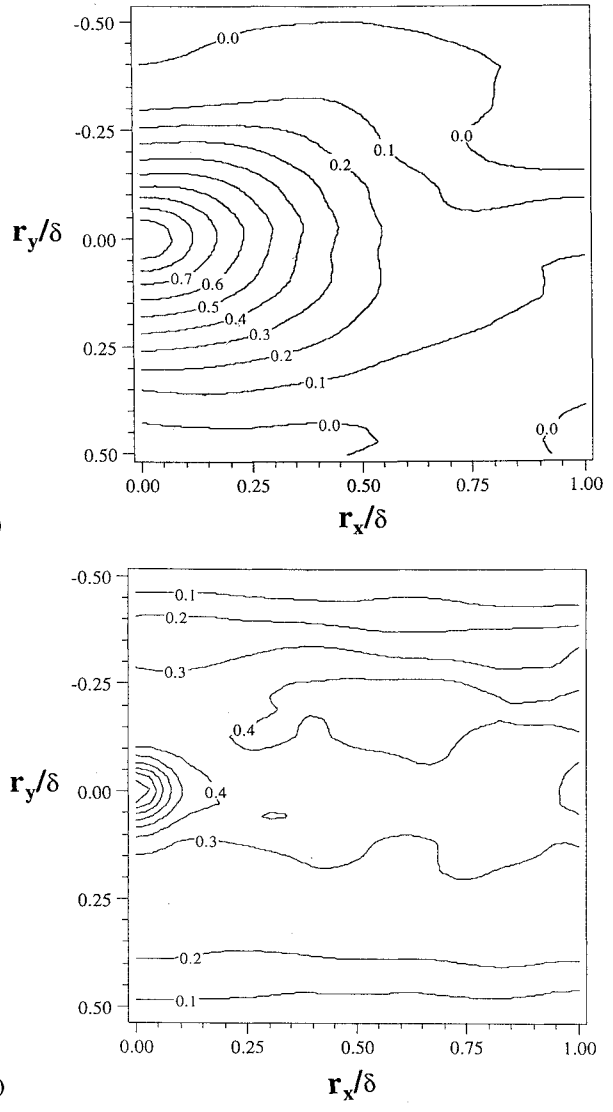

Fig. 12 Contours of the centerline autocorrelations a) $R_{u'u'}(r_x, r_y, y_{CL}, 0)$ and b) $R_{\omega\omega}(r_x, r_y, y_{CL}, 0)$, showing the average eddy shape, size, and orientation.

The differences between $U_c(y)$ and $U(y)$ are consistent with the spread of data shown by other experimental studies (which include single-stream[1–3,33] and two-stream shear layers[4]).

To determine the average size, shape, and orientation of eddies in the shear layer, the two-dimensional spatial autocorrelation $R_{u'u'}(r_x, r_y, y, 0)$ was calculated at several transverse locations and also averaged across the entire shear layer.[23] Figure 12a shows the contour plot for the centerline transverse position, showing only the right-half-plane, since this correlation is an odd function. We see that the average eddy is elliptical and elongated in the streamwise direction, with a ratio of major to minor axes of ~5/3. The streamwise dimension based on the $1/e$ contour is ~33 mm, (i.e., $\Lambda/\delta \sim 0.42$), which agrees well with the present integral scale data (obtained from Fig. 8 but not shown here). Hernan and Jimenez[30] show that for passive scalar visualization of individual eddies in an incompressible flow, the instantaneous angle of the major axis of the eddy with respect to the streamwise direction may be positive or negative and is not necessarily small. Here we find a slight positive angle for the centerline, which is consistent with results of Tung.[34] However, this is inconsistent with the theoretical stress angle of −28 deg, a disparity also noted by Tung. We also noted that at transverse positions of $\eta = 0.5$ and −0.5, the correlation angle was strongly positive and negative, respectively, whereas integration over all transverse positions yielded a near zero inclination angle,[23] which is essentially consistent with Koochesfahani et al.[24]

Figure 12b shows the centerline two-dimensional spatial autocorrelation of instantaneous vorticity, $R_{\omega\omega}(r_x, r_y, y_{CL}, 0)$, where we

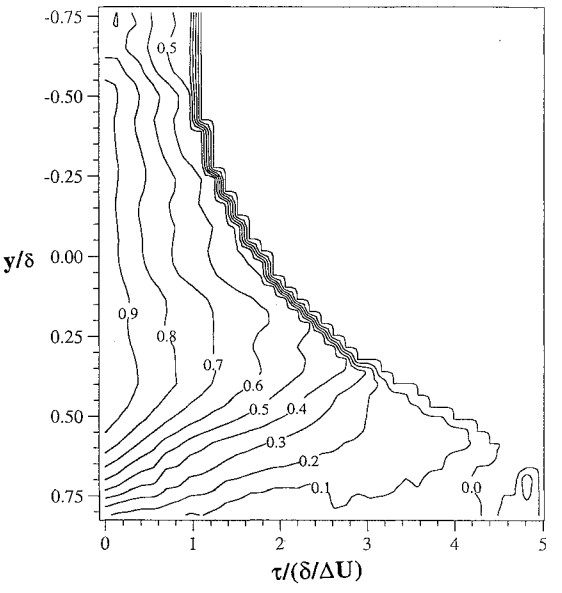

Fig. 13 Lagrangian correlation (using Taylor's hypothesis) of streamwise velocity fluctuations.

again note a small positive angle of inclination. The much reduced extent of the correlation in both directions (as compared with Fig. 12a) is consistent with the observed small-scale structure in Figs. 2 and 3 (and inferred in Fig. 10). This again shows that a point vortex model with peak vorticity in the center of an eddy and a radially monotonically decreasing distribution of width δ is an inaccurate description of actual vorticity distribution in a high-Reynolds-number turbulent free shear layer.

Finally, we may also estimate the Lagrangian eddy lifetime based on streamwise velocity fluctuations. Previously, such an estimation was typically made using the Taylor hypothesis such that the velocity of the perturbation between the streamwise probe positions r_x would (on average) be approximately equal to $U(y)$. From this, the moving frame temporal correlation is given as $R_{u'u'}(r_x, 0, y, \tau)$, where for this correlation $r_x = U(y)\tau$. Such a distribution can be seen in Fig. 13 for the present data, where τ is restricted to integral multiples of the interframe time period ($\Delta t''$). The immediate dropoff of the correlation in a hyperbolic tangent profile is simply related to the specification of a zero value for points that convected out of the finite streamwise domain. The high-speed region is on top (negative y/δ) and the low-speed region is on the bottom (positive y/δ), and so we see that the "border" shape is basically a reciprocal function of the mean velocity profile. The qualitative timescales taken from this plot show a longer persistence of fluctuations in the middle to low-speed side of the shear layer. Also, note that the correlation remains strong (~0.5) even as the fluid particles convect out of our field of view, despite a streamwise offset $r_x/\delta \sim 1.5$. Points near the edge of the shear layer are at best qualitative due to increased intermittency and higher relative error in the correlation values.

Given the unique detailed temporal and spatial resolution available with the present PIV technique, we may also compute a Lagrangian temporal correlation $R_{u'u'}(r_x, r_y, y, \tau)$ based on tracking the fluid particles motion. This is done herein by updating the correlation point of interrogation for each frame as follows:

$$r_x = x_N - x, \qquad r_y = y_N - y, \qquad \tau = t_N - t \tag{5}$$

where

$$x_i = x_{i-1} + u(x_{i-1}, y_{i-1}, t_{i-1})^* \Delta t''$$

$$y_i = y_{i-1} + v(x_{i-1}, y_{i-1}, t_{i-1})^* \Delta t''$$

$$t_i = t_{i-1} + \Delta t''$$

where $x_0 = x$, $y_0 = y$, and N is the total number of frames taken from the initial point in time t, i.e., $\tau = N^* \Delta t''$. This formulation uniformly applied to a finite domain is inherently biased towards

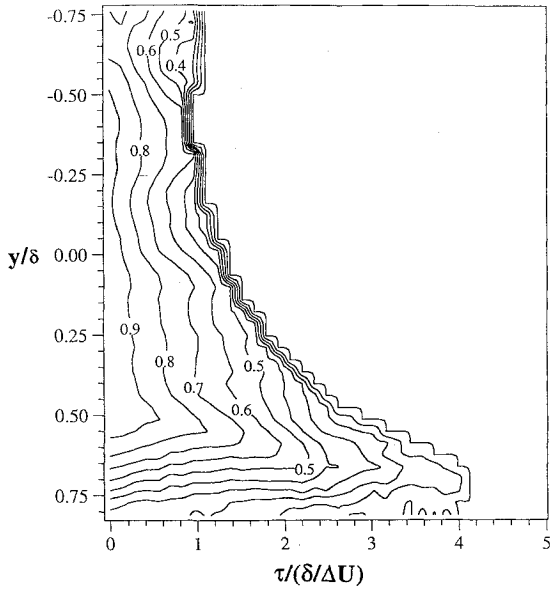

Fig. 14 Lagrangian correlation (without Taylor's hypothesis) of streamwise velocity fluctuations.

inclusion of initially negative u' values, since such fluid particles will remain in the field of view for a longer time and will be sampled more times. To eliminate this strong bias, correlation pairs are not considered when τ is greater than the minimum time taken for one of the fastest moving fluid particles [at speed $U(y) + 2u'_{\text{rms}}(y)$] to convect out of the field of view from its initial streamwise position. The resulting correlation in Fig. 14 maintains a similar shape as in Fig. 13 but only predicts longer eddy lifetimes than the Taylor hypothesis correlation in a small portion of the low-speed side. The reason for the typical reduced correlation stems from the importance of the large-scale structures. Consider a simple large eddy where we initiate our correlation point on the top portion (close to the high-speed stream). At this instant, we may expect a positive u'. However, as the eddy convects, the rotational component will move this fluid particle clockwise to the bottom of the eddy where the streamwise perturbation is likely to be negative. Therefore, using the instantaneous velocity yields a more accurate description of the local translational velocity, but if the tracking point is not in the center of the eddy, it will be contaminated with the rotational velocity component that can change the velocity perturbation.

Conclusions

The spatially and temporally resolved velocity field of a high-Reynolds-number, two-stream, planar, turbulent free shear layer was obtained using cinematic PIV. This is the first such experimental data obtained for shear layers, although instantaneous velocity fields have been obtained in low-Reynolds-number experiments. The present shear layer has a velocity ratio of 0.23 and a Reynolds number based on velocity thickness and ΔU of 2.62×10^4. A simple optimization of the PIV parameters was completed to allow high spatial and temporal resolution while minimizing the maximum expected velocity uncertainty (2.1%).

The structure of the shear layer was very different from that seen in previous low-Reynolds-number shear layers in that, instead of a classical eddy/braid structure, complex three-dimensional clusters with vortices of both signs were observed. The velocity field evolution was also notably different from that of the passive scalar field, where the former exhibited stronger temporal variations and reduced spatial coherency. Eddy agglomeration yielded significant substructure, while eddy tearing (large eddies straining smaller eddies into braids) was noted frequently.

The time-shifted spatial correlation was performed to obtain the convection velocity based on both u' and vorticity, which had not been previously done. These two correlations displayed very similar results, as well as consistency with previous studies. The two-dimensional spatial autocorrelation showed an average eddy shape both at the centerline as well as integrated over the whole shear layer as elliptical with no significant mean angle of the major axis to the streamwise direction. The autocorrelation of vorticity indicated a much smaller structure than that associated with u', consistent with DNS results. Finally, the moving frame temporal correlation based on u' was performed first by employing Taylor's hypothesis and second based on integration of actual instantaneous velocities. Both correlations are still fairly strong at most transverse locations by the time the fluid particles convect out of the field of view, but the Taylor hypothesis generally predicts longer eddy lifetimes than the Lagrangian tracking correlation, due to effects of eddy rotation on the sign of u'.

Acknowledgments

This work was supported by the Office of Naval Research under Contract N00014-92-J-1157 with Edwin Rood as technical monitor. We wish to acknowledge the PIV expertise of Carl Meinhart as well as the assistance of Greg Lundstrum and Barry Ford.

References

[1]Davies, P. O. A. L., Fisher, M. J., and Barratt, M. J., "The Characteristics of the Turbulence in the Mixing Region of a Round Jet," *Journal of Fluid Mechanics*, Vol. 15, 1963, pp. 337–367.

[2]Wygnanski, I., and Fiedler, H. E., "The Two-Dimensional Mixing Region," *Journal of Fluid Mechanics*, Vol. 41, No. 2, 1970, pp. 327–361.

[3]Batt, R. G., "Turbulent Mixing of Passive and Chemically Reacting Species in a Low-Speed Shear Layer," *Journal of Fluid Mechanics*, Vol. 82, No. 1, 1977, pp. 53–95.

[4]Jones, B. G., Planchon, H. P., and Hammersley, R. J., "Turbulent Correlation Measurements in a Two-Stream Mixing Layer," *AIAA Journal*, Vol. 11, No. 8, 1973, pp. 1146–1150.

[5]Spencer, B. W., and Jones, B. G., "Statistical Investigation of Pressure and Velocity Fields in the Turbulent Two-Stream Mixing Layer," AIAA Paper 71-613, June 1971.

[6]Balint, J.-L., and Wallace, J. M., "The Statistical Properties of the Vorticity Field of a Two-Stream Turbulent Mixing Layer," *Advances in Turbulence 2*, edited by Fernholz and Fiedler, Springer–Verlag, Berlin, 1989, pp. 74–78.

[7]Foss, J. F., and Haw, R. C., "Vorticity and Velocity Measurements in a 2:1 Mixing Layer," *Forum on Turbulent Flows*, edited by Bower, Morris, and M. Samimy, American Society of Mechanical Engineers: Fluids Engineering Div., Vol. 94, 1990, pp. 115–120.

[8]Brown, G. L., and Roshko, A., "On Density Effects and Large Structure in Turbulent Mixing Layers," *Journal of Fluid Mechanics*, Vol. 64, No. 4, 1974, pp. 775–816.

[9]Dimotakis, P. E., "Turbulent Free Shear Layer Mixing and Combustion," *High-Speed Flight Propulsion Systems*, edited by S. N. B. Murthy and E. T. Curran, Vol. 137, Progress in Astronautics and Aeronautics, AIAA, Washington, DC, 1991, pp. 265–340.

[10]Fiedler, H. E., "Transport of Heat Across a Plane Turbulent Mixing Layer," *Advances in Geophysics*, Vol. 18, 1974, pp. 93–109.

[11]Adrian, R. J., "Particle-Imaging Techniques for Experimental Fluid Mechanics," *Annual Review of Fluid Mechanics*, Vol. 23, 1991, pp. 261–304.

[12]Gray, C., Greated, C. A., McCluskey, D. R., and Easson, W. J., "An Analysis of the Scanning Beam PIV Illumination System," *Engineering Optics*, Vol. 2, 1991, pp. 461–468.

[13]Rockwell, D., Magness, C., Towfighi, J., Akin, O., and Corcoran, T., "High Image-Density Particle Image Velocimetry Using Laser Scanning Techniques," *Experiments in Fluids*, Vol. 14, 1993, pp. 181–192.

[14]Dimotakis, P. E., Debussy, F. D., and Koochesfahani, M. M., "Particle Streak Velocity Field Measurements in a Two-Dimensional Mixing Layer," *Physics of Fluids*, Vol. 24, No. 6, 1981, pp. 995–999.

[15]Post, M. E., Trump, D. D., Goss, L. P., and Hancock, R. D., "Two-Color Particle-Imaging Velocimetry Using a Single Argon-Ion Laser," *Experiments in Fluids*, Vol. 16, 1994, pp. 263–272.

[16]Vogel, A., and Lauterborn, W., "Time-Resolved Particle Image Velocimetry Used in the Investigation of Cavitation Bubble Dynamics," *Applied Optics*, Vol. 27, No. 9, 1988, pp. 1869–1876.

[17]Stolz, W., Köhler, J., Lawrenz, W., Meier, F., Bloss, W. H., Maly, R. R., Herweg, R., and Zahn, M., "Cycle Resolved Flow Field Measurements Using a PIV Movie Technique in a SI Engine," Society of Automotive Engineers, SAE Paper 922354, 1992.

[18]Lin, J. C., and Rockwell, D., "Cinematographic System for High-Image-Density Particle Image Velocimetry," *Experiments in Fluids*, Vol. 17, 1994, pp. 110–114.

[19]Willert, C. E., and Gharib, M., "Digital Particle Image Velocimetry," *Experiments in Fluids*, Vol. 10, 1991, pp. 181–193.

[20]Huang, H. T., Fiedler, H. E., and Wang, J. J., "Limitation and Improvement of PIV, Part II: Particle Image Distortion, a Novel Technique," *Experiments in Fluids*, Vol. 15, 1993, pp. 263–273.

[21]Dimotakis, P. E., and Brown, G. L., "The Mixing Layer at High Reynolds Number: Large-Structure Dynamics and Entrainment," *Journal of Fluid Mechanics*, Vol. 78, No. 3, 1976, pp. 535–560.

[22]Cebrzynski, M. S., "Turbulence Modulation of a Bubbly Free Shear Layer," M.S. Thesis, Univ. of Illinois at Urbana–Champaign, Urbana, IL, 1994.

[23]Oakley, T. R., "A Cinematic Particle Image Velocimetry Study of Bubble Dispersion in a Turbulent Free Shear Layer," M.S. Thesis, Univ. of Illinois at Urbana–Champaign, Urbana, IL, 1995.

[24]Koochesfahani, M. M., Catherasoo, C. J., Dimotakis, P. E., Gharib, M., and Lang, D. B., "Two-Point LDV Measurements in a Plane Mixing Layer," *AIAA Journal*, Vol. 17, No. 12, 1979, pp. 1347–1351.

[25]Keane, R. D., and Adrian, R. J., "Optimization of Particle Image Velocimeters: Part II. Multiple Pulsed Systems," *Measurement Science Technology*, Vol. 2, 1991, pp. 963–974.

[26]Keane, R. D., and Adrian, R. J., "Theory of Cross-Correlation Analysis of PIV Images," *Applied Scientific Research*, Vol. 49, 1992, pp. 191–215.

[27]Prasad, A. K., Adrian, R. J., Landreth, C. C., and Offutt, P. W., "Effect of Resolution on the Speed and Accuracy of Particle Image Velocimetry Interrogation," *Experiments in Fluids*, Vol. 13, 1992, pp. 105–116.

[28]Meinhart, C. D., Prasad, A. K., and Adrian, R. J., "A Parallel Digital Processor System for Particle Image Velocimetry," *Measurement Science Technology*, Vol. 4, 1993, pp. 619–626.

[29]Moffat, R. J., "Contributions to the Theory of Single-Sample Uncertainty Analysis," *Journal of Fluids Engineering*, Vol. 104, 1982, pp. 250–258.

[30]Hernan, M. A., and Jimenez, J., "Computer Analysis of a High-Speed Film of the Plane Turbulent Mixing Layer," *Journal of Fluid Mechanics*, Vol. 119, 1982, pp. 323–345.

[31]Rogers, M. M., and Moser, R. D., "Direct Simulation of a Self-Similar Turbulent Mixing Layer," *Physics of Fluids*, Vol. 6, No. 2, 1994, pp. 903–923.

[32]Lasheras, J. C., and Choi, H., "Three-Dimensional Instability of a Plane Free Shear Layer: An Experimental Study of the Formation and Evolution of Streamwise Vortices," *Journal of Fluid Mechanics*, Vol. 189, 1988, pp. 53–86.

[33]Wills, J. A. B., "On Convection Velocities in Turbulent Shear Flows," *Journal of Fluid Mechanics*, Vol. 20, 1964, pp. 417–432.

[34]Tung, A. T.-C., "Properties of Conditional Eddies in Free Shear Flows," Ph.D. Thesis, Univ. of Illinois at Urbana–Champaign, Urbana, IL, 1982.